

Alma Mater Studiorum Università di Bologna
Archivio istituzionale della ricerca

Tuning the Electro-Optical Properties of Mixed-Halide Trityl Radicals Bearing para-Brominated Positions through Halogen Substitution

This is the final peer-reviewed author's accepted manuscript (postprint) of the following publication:

Published Version:

Mesto, D., Dai, Y., Dibenedetto, C.N., Punzi, A., Krajcovic, J., Striccoli, M., et al. (2023). Tuning the Electro-Optical Properties of Mixed-Halide Trityl Radicals Bearing para-Brominated Positions through Halogen Substitution. EUROPEAN JOURNAL OF ORGANIC CHEMISTRY, 26(1), 1-8 [10.1002/ejoc.202201030].

Availability:

This version is available at: <https://hdl.handle.net/11585/913164> since: 2023-01-31

Published:

DOI: <http://doi.org/10.1002/ejoc.202201030>

Terms of use:

Some rights reserved. The terms and conditions for the reuse of this version of the manuscript are specified in the publishing policy. For all terms of use and more information see the publisher's website.

This item was downloaded from IRIS Università di Bologna (<https://cris.unibo.it/>).
When citing, please refer to the published version.

(Article begins on next page)

This is the final peer-reviewed accepted manuscript of:

D. Mesto, Y. Dai, C. N. Dibenedetto, A. Punzi, J. Krajčovič, M. Striccoli, **F. Negri**, D. Blasi "Tuning the Electro-Optical Properties of Mixed-Halide Trityl Radicals Bearing para-Brominated Positions through Halogen Substitution", *Eur. J. Org. Chem.*, **2023**, 26, e202201030. DOI: 10.1002/ejoc.202201030.

The final published version is available online at:

<https://doi.org/10.1002/ejoc.202201030>

Terms of use:

Some rights reserved. The terms and conditions for the reuse of this version of the manuscript are specified in the publishing policy. For all terms of use and more information see the publisher's website.

Tuning the Electro-Optical Properties of Mixed-Halide Trityl Radicals Bearing para-Brominated Positions through Halogen Substitution

Davide Mesto,^[a] Yasi Dai,^[b] Carlo N. Dibenedetto,^{[a][c]} Angela Punzi,^[a] Jozef Krajčovič,^{[a][d]} Marinella Striccoli,^[c] Fabrizia Negri,^{[b]*} and Davide Blasi^{[a]*}

[a] D. Mesto, Prof. A. Punzi, C.N. Dibenedetto, Dr. D. Blasi*

Dipartimento di Chimica
Università degli Studi di Bari "Aldo Moro"
Via Orabona 4, 70125 – Bari, Italy
E-mail: davide.blasi@uniba.it

[b] Y. Dai, Prof. F. Negri

Dipartimento di Chimica "Giacomo Ciamician",
Università degli Studi di Bologna and INSTM UdR Bologna,
40126 - Bologna, Italy
E-mail: fabrizia.negri@unibo.it

[c] C.N. Dibenedetto, Dr. M. Striccoli

CNR-Istituto per i Processi chimico Fisici (CNR-IPCF), SS Bari,
Via Orabona 4, 70125 – Bari, Italy

[d] Prof. J. Krajčovič

Faculty of Chemistry, Materials Research Centre
Brno University of Technology,
Purkyňova 464/118, 612 00 Brno, Czech Republic

Supporting information for this article is given via a link at the end of the document.

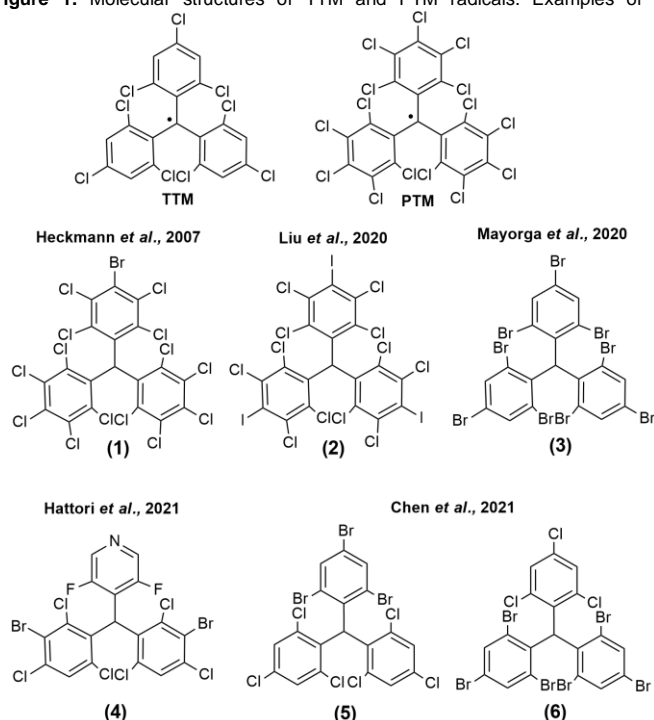
Abstract: In this work, the synthesis and characterization of two new trityl radicals bearing two *p*-brominated positions, *i.e.* the 2,2'-((perchlorophenyl)methylene)bis(1,3,5-tribromobenzene) radical and the 6,6'-((perchlorophenyl)methylene)bis(3-bromo-1,2,4,5-tetrafluorobenzene) radical, are presented. Slightly modifying the strategy typically used for the synthesis of non-symmetric mixed-halide trityl radicals, we were able to considerably increase the reaction yield for the radical precursors. In addition, for the first time the electro-optical properties of a highly fluorinated trityl radical were studied, achieving the most blue-shifted emission for a trityl radical reported up to now. Quantum-chemical calculations carried out to supplement the experimental investigation, support the electrochemical and spectroscopic data and rationalize the observed blue shift of the highly fluorinated species.

Introduction

Inert triaryl methyl radicals are getting an increasing interest in several technological fields since they offer the possibility of combining several features within a single chemical species, representing the perfect building block in the design of multifunctional molecular materials.^[1] Recently, they are getting noticed for their unique optical properties^[2] such as: emission in the first biological window (650 - 950 nm),^[3,4] circularly polarized luminescence (CPL),^[5-7] two-photon absorption,^[8,9] excimer formation and magnetoluminescence^[10-12] and the possibility to obtain the 100% of internal quantum efficiency in electroluminescence devices.^[13-15] Due to this rising interest, the synthesis of new doublet emitters is of extreme relevance.^[16] The two most studied polychlorinated trityl radicals, *i.e.* the tris(2,4,6-trichlorophenyl)methyl (TTM) and tri(perchlorophenyl)methyl radical (PTM) radicals (Figure 1), can be easily synthesized via a

single-step Friedel-Craft reaction between chloroform and the corresponding chlorobenzene using AlCl₃ as catalyst.^[17,18] The reaction is performed at a temperature higher than the melting

Figure 1. Molecular structures of TTM and PTM radicals. Examples of



polyhalogenated triaryl methane derivatives bearing brominated or iodinated positions.

point of the halobenzene since it works both as reactant and solvent and for this reason it is used in excess. The resulting polychlorinated triphenylmethanes are then converted in the

corresponding carbanions treating with a base (usually tetrabutylammonium hydroxide) and subsequently oxidized to give radicals. Unfortunately, **TTM** and **PTM** structures offer a poor chemical versatility due to the lower reactivity of chlorine atoms compared with bromine and iodine ones. Although some functionalization have been reported involving directly chlorinated substrates,^[7,19] many efforts have been tried to increase the reactivity of polyhalogenated triphenyl methane adducts (radical precursors) by introducing bromine or iodine substituents in different positions (**Figure 1**).^[4,5,20–22] In fact, such substrates can be easily functionalized *via* transition-metal mediated cross-coupling reactions expanding their chemical versatility. Without going into the synthetic details of each example reported in **Figure 1**, in general their synthesis is not trivial, especially in the case of bis- and tris- *p*-substituted adducts. In this context, the design of a simple and high-yielding synthesis for these species is highly desirable.

In this work, the synthesis of new polyhalogenated triphenylmethanes bearing two *p*-brominated positions is presented (derivatives **7** and **8** in **Figure 2**). Friedel-Crafts reactions using the 1,2,3,4,5-pentachlorobenzene (**PCB**) as substrate were used, varying the haloalkane (CHCl_3 vs. CHBr_3), the catalyst (AlCl_3 vs. AlBr_3), and the halobenzene (1,3,5-tribromobenzene (**TBB**) vs. 1-bromo-2,3,5,6-tetrafluorobenzene (**Br4FB**)). The focus on *p*-substituted cores is due to the higher photoluminescence quantum yields (PLQYs) generally displayed by push-pull trityl radicals coupled through *para* positions.^[21] The two radical precursors **7** and **8** were then converted into the corresponding radical species (**12** and **13** in **Scheme 2**), for addressing the role played by the different halogen substitution (Br vs. F) on the optical and electrochemical properties. These two new radical precursors represent promising candidates for the synthesis of new derivatives for different applications. In fact, while the high *ortho*-hindrance of **7** can be exploited for the synthesis of radicals suitable for CPL applications, due to the enhancement of the racemization barrier between the *Plus* and *Minus* atropoisomers,^[5,6] the derivative **8** can be used in the synthesis of new green-yellow radical emitters, thanks to the strong inductive effect exerted by the eight fluorine substituents,^[23–25] and their steric effects on the molecular geometry.

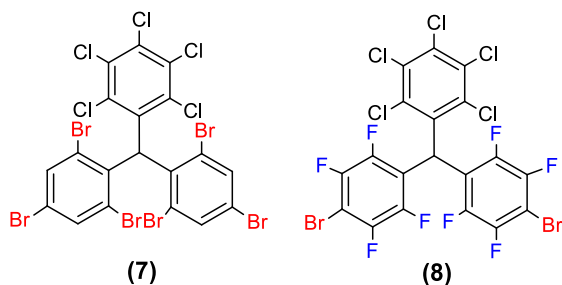
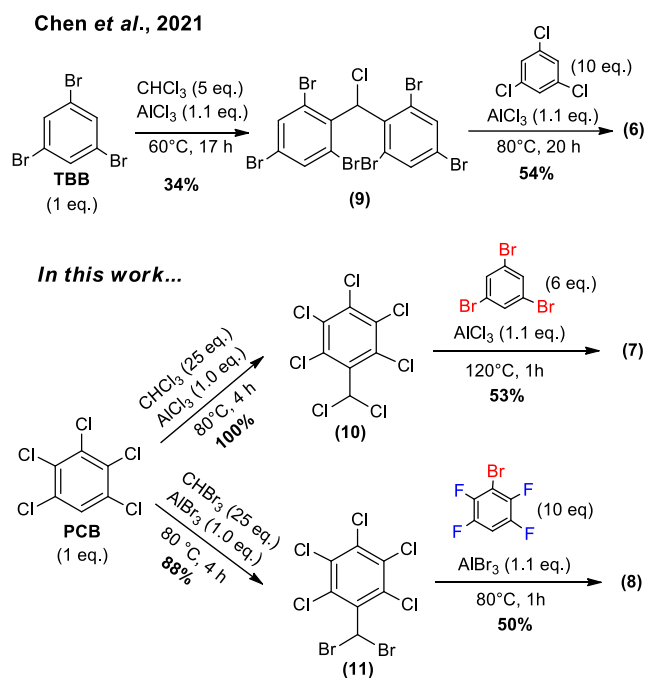


Figure 2. Molecular structures bis-*p*-brominated polyhalogenated triphenylmethane synthesized in this work.

The strategy used for the synthesis of bis-*p*-brominated triphenylmethanes was based on the approach developed by Chen and co-workers^[22] for the synthesis of **6** (**Scheme 1**), which consisted in multistep Friedel-Craft reactions. The bottleneck of their approach was represented by the synthesis of the intermediate **9**, in which chloroform was used in a large excess (both as reactant and solvent). In these conditions, the **TBB** can be methylated in more than one position, leading to several biproducts. This problem can be easily overcome inverting the order of the two Friedel-Craft reactions and using the **PCB** as substrate (**Scheme 1**). The main advantage of using **PCB** is that this substrate can be methylated just in one position, hence higher temperatures and a strong excess of haloalkane can be used without to give any biproduct and making the reaction faster. In fact, the 1,2,3,4,5-pentachloro-6-(dichloromethyl)benzene **10** and the 1,2,3,4,5-pentachloro-6-(dibromomethyl)benzene **11** were obtained in quantitative and excellent yield using $\text{CHCl}_3/\text{AlCl}_3$ and $\text{CHBr}_3/\text{AlBr}_3$, respectively. The two intermediates were used in a second Friedel-Craft reaction with an excess of **TBB** and **Br4FB** at 120°C and 80°C respectively, to give the two radical precursors **7** and **8**. With this simple change it was possible to considerably improve the reaction yield (2.9 times for **7** and 2.4 times for **8** compared to **6**) and reduce the reaction time (37 h vs. 5 h). In the synthesis of **7**, the temperature of 120°C represents the minimum value suited for this reaction, in order to melt the excess of **TBB**, that acts as reagent and solvent. The elevated temperature needed for this reaction could be a critical issue, because of the electron deficient character of polyhalogenated benzenes. In fact, it is reported that, for temperature higher than 80°C, the Cl^- and Br^- anions can lead to nucleophilic aromatic substitution, affording biproducts that cannot be separated *via* column chromatography neither by crystallization.^[5,22] However, under the experimental conditions reported in the **Scheme 1**, we observed the formation



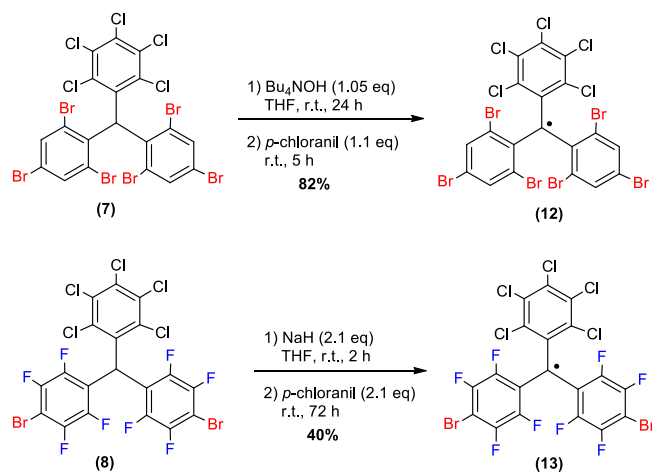
of **7** with a good purity (**Figure S3**).

Scheme 1. Synthetic route to radical precursors **7** and **8**.

Attempts to synthesize **7** starting from **11** and **TBB** in the presence of AlBr_3 at 120°C resulted in lower yield (14%) and

Results and Discussion

purity (**Scheme S1**). This behavior was already observed in the synthesis of **3**,^[5] and it was attributed to the high rotation barrier generated by the presence of the two bromine substituent on the methyl unit, which make extremely difficult the formation of the coplanar benzylic carbocation, making the reaction slower.^[26–28] The radical precursor **8** was synthesized to a temperature of 80 °C (no reaction took place below this temperature), allowing to minimize the formation of biproducts given by nucleophilic aromatic substitutions (**Figure S4**). Reaction of **10** with **Br4FB** in the presence of AlCl_3 at 80 °C also afforded compound **8** in comparable yield (50%) but with a lower purity (**Scheme S1**). The higher electron-deficient nature of **Br4FB** compared to **TBB**, makes compound **8** more prone to nucleophilic aromatic substitution, even if a lower temperature of 80 °C was used. In this case, the reaction time was limited to one hour to limit the formation of biproducts hard to remove *via* chromatography. Unfortunately, a reaction time of one hour was not sufficient to have the complete conversion of **11** into **8**, negatively affecting the reaction yield. Compounds **7** and **8** were converted into radicals **12** and **13**, respectively, as shown in **Scheme 2**. A slight excess of tetrabutylammonium hydroxide in anhydrous THF was used for the conversion of **7** into the corresponding anion, which was then oxidized with *p*-chloranil leading to **12** in 82% yield. The same synthetic approach revealed ineffective for the preparation of radical **13**, since a complex mixture of products is formed when **8** was treated first with tetrabutylammonium hydroxide and then with *p*-chloranil. Treatment of **8** with an excess of NaH (2.1 eq) as the base, followed by oxidation of resulting anion with *p*-chloranil led to radical **13** in 40% yield (a not trivial chromatographic purification is needed to separate **13** from its precursor and other minor radical biproducts). The use of stoichiometric amount of NaH resulted in lower conversion of **8** into the radical **13**, with a considerable amount of **8** still present in the crude product. The use of a larger excess of base (3.7 eq.), or the substitution of *p*-chloranil with AgNO_3 as oxidant, did not determine an improvement of the reaction yield (**Table S1**). The lack of the full conversion of **8** into the corresponding anion using even an excess of a strong base such as NaH, is not fully understood and it is currently under investigation.



Scheme 2. Synthetic approaches to radicals **12** and **13**.

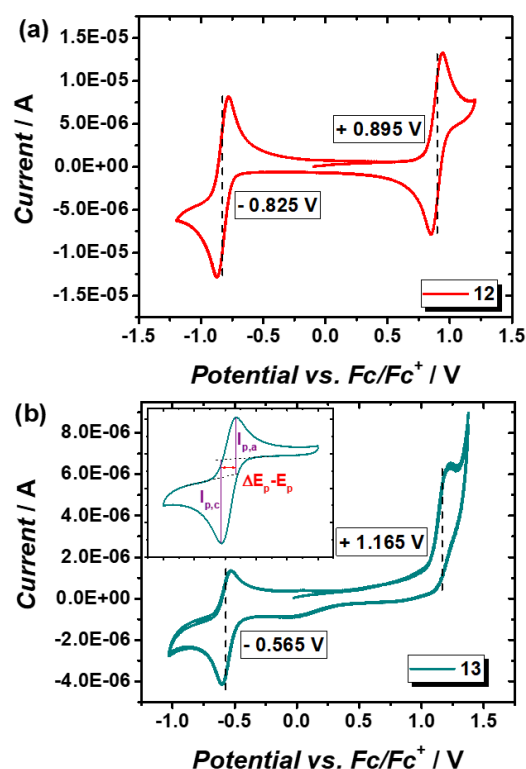


Figure 3. Cyclic voltammograms of radical **12** (a) and radical **13** (b) with 0.1M of $\text{N}(\text{Bu})_4\text{PF}_6$ in CH_2Cl_2 , at the scan rate of 0.1 V/s. The inset shows in detail the non-completely reversible redox behavior of radical **13**.

Moving to the electrochemical characterization, the cyclic voltammograms of the two radicals are reported in **Figure 3**.

Analyzing the voltammogram of the radical **12**, two reversible redox couples are observed at $-0.825 \text{ V vs. Fc/Fc}^+$ and $0.895 \text{ V vs. Fc/Fc}^+$, related to the formation of the carbanion and carbocation, respectively. In contrast, radical **13** shows a quasi-reversible redox couple associated to the formation of the carbanion at $-0.565 \text{ V vs. Fc/Fc}^+$, with a ratio between the cathodic and anodic current $I_{p,c}/I_{p,a}$ (inset **Figure 3b**) of 1.38. For the polyfluorinated radical it is difficult to determine the reversibility for the formation of its carbocation species since the potential is shifted to ca. $1.165 \text{ V vs. Fc/Fc}^+$. What is clear is that the presence of eight fluorine atoms considerably increases the electron-acceptor character of the radical **13** compared to **12**, shifting the potential for the formation of the carbanion of 0.260 V. In both cases (radicals **12** and **13**) the $\Delta E_p - E_p$ between the potentials of the cathodic and anodic peaks was of 90 mV.

The electrochemical data can be rationalized based on molecular orbitals (MOs) computed at the ground state equilibrium structure of **12** and **13** (**Figures S7–S8**). To better understand the changes in shape and energy of MOs when moving from **12** to **13**, it is important to also consider the differences in computed ground state geometries. Notably, the twisting angles of the substituted phenyl rings in **12** and **13** are remarkably different (**Scheme S2**). While the three phenyl rings of **12** display similar twisting angles, the two fluorinated phenyl rings in **13** are less twisted, at the expenses of a remarkably larger twist of the chlorinated ring probably due to a repulsive effect of *ortho* fluorine atoms on the nearby phenyl rings (**Figure S9**). The reduced twisting of fluorinated rings also suggests an increased conjugation efficiency with the central carbon, at the expenses of the chlorinated phenyl. Remarkably, these geometrical features are reflected in the shape of the SOMO/SUMO orbitals in **Figure 4**.

The reduced conjugation combined with unfavorable level alignment of the chlorinated ring in **13**, is reflected in SOMO and SUMO orbitals where the electron density extends beyond the central carbon, toward the two fluorinated phenyls with only a modest contribution of the third, perchlorinated ring. In contrast, the SOMO and SUMO orbitals of **12** display an almost identical extension on the three phenyl rings. At the same time, the electron-acceptor character of fluorine leads to a remarkable energy lowering of the SOMO/SUMO of **13** compared to **12**. Note that similar effects are predicted by B3LYP/6-31+G** (**Figure 4**) and ω B97X-D/6-31+G** calculations. The observed changes in redox potentials can thus be rationalized by comparison with computed orbital energies. The lowering of the SOMO from -6.06 eV for **12** to -6.32 eV for **13** agrees with the reported increase from 0.895 V to 1.165 V of the redox potential for the formation of the cation. Similarly, the reported change of redox potential for the formation of the carbanion is supported by the lowering of the SUMO energy, from -3.86 eV (**12**) to -4.20 eV (**13**). As noted above, the remarkable lowering of the SOMO and SUMO energy can be rationalized by the increased contribution of fluorinated phenyl rings to these orbitals, driven by the increased conjugation associated to the reduced twisting of the two phenyl rings.

The absorption spectra of the two radicals in chloroform and cyclohexane are reported in **Figure 5**. As already observed for other triarylmethyl radicals, the introduction of fluorine atoms in the structure induces a blue shift of the absorption and a lowering of the molar extinction coefficient.^[23] The absorption maximum in chloroform shifts from the 390 nm ($\epsilon = 28600 \text{ M}^{-1}\text{cm}^{-1}$) of **12** to the 351 nm ($\epsilon = 15970 \text{ M}^{-1}\text{cm}^{-1}$) of **13** (blue-shift of 0.355 eV). Same trend can be observed for the weak absorption band in the visible, peaked at 561 nm ($\epsilon = 940 \text{ M}^{-1}\text{cm}^{-1}$) and 539 nm ($\epsilon = 540 \text{ M}^{-1}\text{cm}^{-1}$) for **12** and **13** (blue-shift of 0.090 eV), respectively. Both radicals are fluorescent (**Figure 5b**), without showing any significant solvatochromism. The maximum of the emission for the radical **12** is at 601 nm (Stokes' shift of 0.147 eV) while in the case of **13** the emission is blue shifted at 558 nm (Stokes' shift of 0.078 eV). For both molecules a vibronic transition at low energy is present, that results more intense in chloroform. Interestingly, the radical **13** shows the most blue-shifted emission among all the emitting trityl radicals.^[16] Hence, polyfluorinated radicals can be interesting

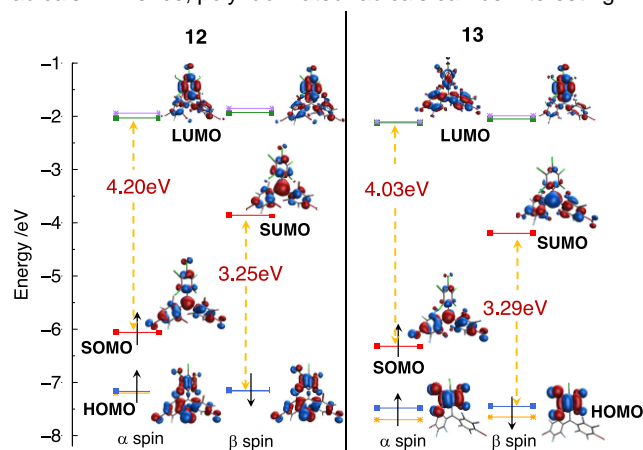


Figure 4 Schematic representation of the B3LYP/6-31+G** molecular orbital energies and shapes of **12** and **13** at their ground state geometry.

candidates for the synthesis of green-emitting doublet species. In this context, the synthesis of new derivatives obtained coupling polyfluorinated trityl cores with electron-withdrawing groups can

be the most effective strategy for obtaining highly fluorescent species in the spectral range across the green and yellow regions. However, the absolute quantum yield (PLQY) for both the radicals remains low, around 1%. In addition, both species shows a severe photobleaching when irradiated with UV-light. A promising solution for the enhancement of both PLQY and photostability could be offered by the presence of *p*-brominated positions. In fact, they can be exploited to couple, *via* transition metal-mediated cross-coupling reactions, the radical core (electron acceptor unit) with weak donor groups, as suggested by recent computational studies^[29] and as already experimentally observed in the case of TTM-carbazole derivative having electron-withdrawing groups on the donor moiety.^[16]

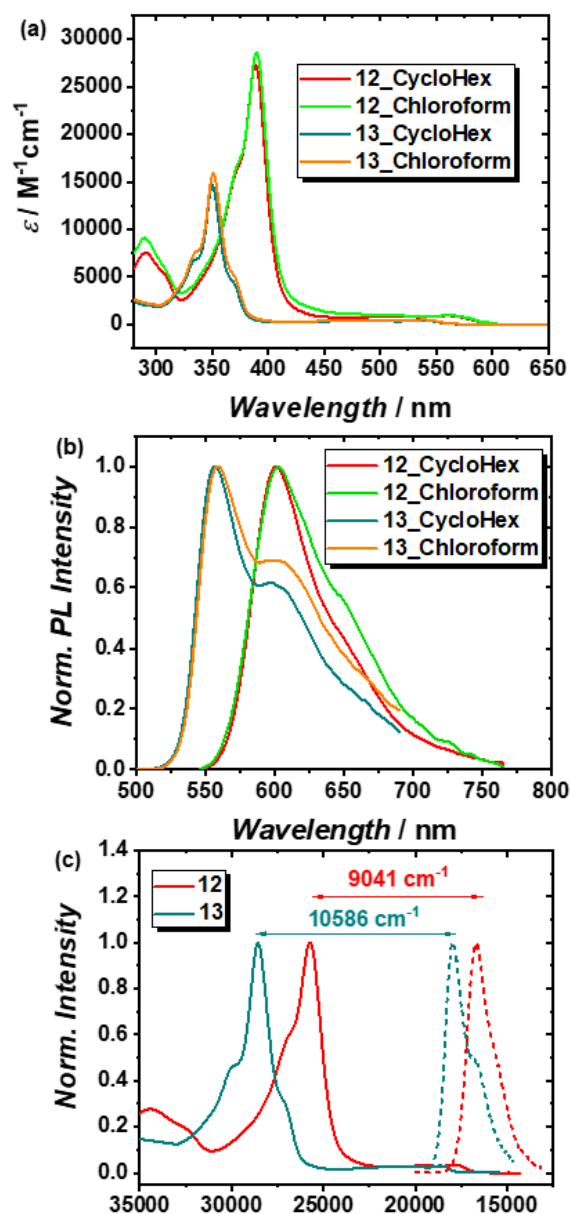


Figure 5. (a) Molar extinction coefficient for radicals **12** and **13** in cyclohexane and chloroform. (b) Normalized PL spectra of radicals **12** and **13** in both solvents, exciting at 350nm and 390nm respectively. (c) Normalized absorption and emission spectra of radicals **12** and **13** in cyclohexane, showing the asymmetric shift of UV and visible bands induced by the fluorine substitutions.

Table 1. Spectroscopic parameters of the two synthesized radicals. The λ_{ex} for emission and PLQY are 350nm and 390nm for radicals **12** and **13**, respectively. The time resolved measurement have been recorded by exciting at 375nm both molecules and the decay profiles have been best fitted with mono-exponential function to estimate the lifetime (τ).

	Solv.	$\lambda_{\text{(abs)}}$ (nm)	ϵ ($\text{cm}^{-1}\text{M}^{-1}$)	$\lambda_{\text{(em)}}$ (nm)	PLQY (%)	τ (ns)
12	CycloHex	389	27650	599	2 \pm 0.4	3.6 \pm 0.2
	CHCl ₃	390	28600	601	1 \pm 0.2	4.2 \pm 0.3
13	CycloHex	350	14660	557	<1 \pm 0.05	1.2 \pm 0.1
	CHCl ₃	351	15970	558	<1 \pm 0.04	1.2 \pm 0.1

Finally, the TCSPC technique allowed us to determine the recombination dynamics of the emission in the two systems, best fitted by mono-exponential functions (**Figure S13**), and to calculate the relative lifetimes that resulted of 1.2 ns, independently of the solvent, for radical **13** and slower, ca. 4 ns, for **12**, slightly dependent on the solvent (**Table 1**). If we compare the absorption and emission spectrum of the two radicals (**Figure 5c**), it is clear that the blue shift induced by the fluorine substitution affects prevalently the UV-band. In fact, while the difference between the maximum of absorption and emission in **12** is of 9041 cm^{-1} (1.12 eV), this value rises to 10586 cm^{-1} (1.31 eV) in the case of **13**. To better understand the nature of this asymmetric shift, excited state quantum-chemical calculations were performed at TDDFT level and supplemented by the geometry optimization of the lowest energy excited state for both radicals. For comparison, similar calculations were carried out for unsubstituted triphenylmethane (TPM) radical (see the SI). TDDFT calculations show that the lowest energy excited state of both **12** and **13** is dominated by the HOMO(β) \rightarrow SUMO(β) excitation while the excited state responsible for the most intense band in the absorption spectra is dominated by the SOMO(α) \rightarrow LUMO(α) excitation (**Tables S2-S4**). Thus, both **12** and **13** are "SUMO" emitters, as most previously investigated neutral organic radicals^[13] in contrast to unsubstituted TPM, whose luminescence has been observed^[30] and, based on the calculations, can be defined a "LUMO emitter" (see also the SI). The predicted TDDFT excitation energies are in good agreement with the observed data (**Figure S14**) and clearly show a blue shift of the two major absorption bands of **13** compared to **12**, with a more marked blue shift of the highest energy band, in agreement with experiment. Specifically, the predicted blue shift of the lowest energy band is 0.12 eV compared to 0.09 eV observed, while the blue shift of the highest energy band is 0.30 eV, very close to the 0.35 eV observed value. Note that calculations nicely also reproduce the weak shoulder on the red side of the most intense absorption band of **13**, which is due to an additional excited state and is not part of the vibronic structure of the intense transition. Similar results are obtained with the long range corrected functional ω B97X-D (**Figure S15**) except for an overestimation of excitation energies which is typical of this functional. The nature of the two bright excited states and specifically the "SUMO emitter" nature of the lowest excited state, can be simply rationalized by considering the energy difference between orbitals involved in the excitation. As shown in **Figure 4** and **Tables S5-S6**, the $\Delta E(\text{LUMO}(\alpha)/\text{SOMO}(\alpha))$ (4.03 eV for **12**, 4.20 eV for **13**) is larger than the $\Delta E(\text{SUMO}(\beta)/\text{HOMO}(\beta))$ (3.29 eV for **12**, 3.25 eV for **13**)

for both **12** and **13**, thereby supporting the "SUMO emitter" nature of the lowest excited. Furthermore, the TDDFT computed blue shift of the highest energy transition of **13** can be related to the blue shift of the $\Delta E(\text{LUMO}(\alpha)/\text{SOMO}(\alpha))$. In contrast, the predicted $\Delta E(\text{SUMO}(\beta)/\text{HOMO}(\beta))$ is almost identical for the two radicals and only slightly smaller for **13** compared to **12**, a result confirmed also with the ω B97X-D functional (see the SI). Thus, the simple picture provided by MO levels does not account for the computed (TDDFT level) and observed blue shift of the lowest energy transition. There are at least two possible explanations for such discrepancy: first, TDDFT calculations suggest that at least another excited configuration contributes to the wavefunction of the D_1 state of **13** (**Table S4**). Second, even assuming the exclusive role of the HOMO(β) \rightarrow SUMO(β) excitation, one has to consider that the optical gap is different from the fundamental gap. Thus, excitation energy is determined not only by MOs energies but also by the repulsive interaction J between the two orbitals involved in the transition (HOMO(β) and SUMO(β)). Specifically, in a configuration interaction formalism, such repulsion contributes with a negative sign^[31] and reduces the excitation energy: $\Delta E(D_0 \rightarrow D_1) \sim \Delta E(\text{SUMO}(\beta)/\text{HOMO}(\beta)) - J$. **Figure 4** shows that these two orbitals are localized on rather different spatial regions in **13** compared to **12**, thereby reducing the magnitude of the repulsive interaction J . The reduced J implies a larger excitation energy of **13** compared to **12**, thereby accounting for the observed (and TDDFT computed) blue shift.

Finally, the onset of the emission energy determined from the optimized geometries of both D_0 and D_1 states (**Figure S16**) is in very good agreement with observed data: 554 nm (computed) vs 557 nm (experimental) for **13** and 571 nm (computed) vs 599 nm (exp) for **12** (see **Table S7**). To analyze the Franck-Condon vibronic structure observed in luminescence spectra we inspect the computed Huang-Rhys S_k parameters for the $D_1 \rightarrow D_0$ transition (**Table S8**, **Figures S17-S18**) which indicate remarkable vibronic activity for a few vibrational modes in the range 1200-1500 cm^{-1} , corresponding mainly to the CC bond stretching connecting the chlorinated ring to the radical center and CC stretchings of the chlorinated ring, namely the molecular moieties undergoing the largest $D_1 \rightarrow D_0$ geometry change for both **12** and **13**. The computed active modes nicely account for the observed vibronic structure in emission, displaying a second weaker maximum separated by ca. 1300-1400 cm^{-1} from the first main emission band (corresponding to the 0-0 vibronic transition).

Conclusions

In conclusion, two new mixed-halide trityl radicals bearing *p*-brominated positions, were synthesized. The two radical precursors were obtained in good yield thanks to the optimization of the synthetic pathway, properly selecting substrates and reaction conditions and limiting the nucleophilic aromatic substitution reactions that typically affects these reactions. The resulting radicals represent interesting species for the synthesis of new doublet emitters, in particular the polyfluorinated one which shows the most blue-shifted emission (557 nm in cyclohexane) among trityl radicals. Quantum-chemical calculations of molecular orbital energies and excited states support the electrochemical and spectroscopic experimental characterization and demonstrate that both radicals are "SUMO emitters" with a blue shifted emission for compound **13**. Interestingly, while the blue

shift of the highest energy band can be rationalized based on MOs energies, the blue shift of the lowest energy band is likely to be due to the more localized character of the MOs of **13**, a result that might be exploited to design organic radicals with further blue shifted emissions.

Experimental Section

General Remarks: Tetrahydrofuran was distilled from sodium benzophenone before use. Other solvents and chemicals were purchased at the highest commercial purity and used without further purification. Preparative column chromatography was performed using Macherey-Nagel silica gel (60, particle size 0.040-0.063 mm). Macherey-Nagel aluminium sheets with silica gel 60 F254 were used for TLC. ^1H NMR spectra were acquired on an Agilent 500 spectrometer at 500 MHz using the CDCl_3 residual proton peak at $\delta = 7.26$ ppm as internal standard. High-resolution mass spectra were acquired with a Shimadzu high-performance liquid chromatography ion trap time-of-flight (LC-IT-TOF) mass spectrometer via direct infusion of the samples by using methanol as the elution solvent (the samples were previously dissolved in THF, and few drops of the THF solution were added to methanol). Melting points were measured with a Stuart Scientific melting point apparatus SMP3. ATR-FTIR spectra were recorded with a Fourier transform infrared Spectrometer Spectrum Two Perkin Elmer spectrophotometer, operating in the range 4000-400 cm^{-1} . Ultraviolet-visible (UV-vis) spectra were recorded with a Shimadzu UV-2401PC spectrophotometer. Fluorescence spectra were acquired by using a Fluorolog 3 spectrofluorometer (HORIBA Jobin-Yvon). Time resolved measurements were performed by Time-Correlated Single Photon Counting (TCSPC) technique, with a FluoroHub (HORIBA Jobin-Yvon). The samples were excited at 375 nm using a picosecond laser diode (NanoLED 375L) with a pulse length of 80 ps at a 1 MHz repetition rate. The PL signals were detected by a picosecond photon counter (TBX ps Photon Detection Module, HORIBA Jobin-Yvon). The temporal resolution of the experimental setup was ~ 200 ps. DAS6 Analysis® software by Horiba was used to fit the decay profiles with mono-exponential function. Absolute quantum yield measurements were obtained utilizing a "Quanta-phi" integrating sphere coated with Spectralons® and mounted in the optical path of the spectrofluorometer, using as excitation source a 450 W xenon lamp coupled with a double-grating monochromator. The cyclic voltammetry (CV) measurements were performed using an Autolab potentiostat (model PGSTAT128N) by Metrohm. A glassy carbon electrode was used as the working electrode. Platinum wires acted as the counter and reference electrodes, together with the redox couple ferrocenium/ferrocene as external standard. The CV profiles were recorded at the rate of 100 $\text{mV}\cdot\text{s}^{-1}$. Tetrabutylammonium hexafluorophosphate in anhydrous dichloromethane (0.1 M) was used as the supporting electrolyte.

1,2,3,4,5-pentachloro-6-(dichloromethyl)benzene (10)^[18,32] A 25 mL two-necked round bottom flask, equipped with a reflux condenser and a magnetic stirrer, was charged with pentachlorobenzene (500 mg, 2 mmol) and chloroform (4 mL, 50 mmol). This mixture was heated to 80 °C, then AlCl_3 (267 mg, 2 mmol) was added. The reaction mixture was stirred for 4 h at 80 °C until it became blue, then it was cooled to room temperature, quenched with a 1N HCl solution and extracted with CHCl_3 (2x30mL). The combined organic phases were washed with brine, dried over anhydrous Na_2SO_4 and the solvent was removed under vacuum. Compound **10** was

obtained with a quantitative yield as a white solid. $R_f = 0.81$ (hexane); m.p. = 111-113 °C (literature: 106-108 °C);^[27] ^1H -NMR (500 MHz, CDCl_3), δ (ppm): 7.59 (s, 1H); ^{13}C -NMR (126 MHz, CDCl_3), δ (ppm): 135.8, 134.8, 134.6, 134.4, 132.2, 130.4, 66.6; FTIR: $\tilde{\nu}_{\text{max}} = 1365, 1355, 1281, 1231, 1211, 961, 775, 760, 709, 675, 613, 607, 504 \text{ cm}^{-1}$.

1,2,3,4,5-pentachloro-6-(dibromomethyl)benzene (11): A 25 mL two-necked round bottom flask, equipped with a reflux condenser and a magnetic stirrer, was charged with pentachlorobenzene (200 mg, 0.8 mmol) and bromoform (1.8 mL, 20 mmol). This mixture was heated to 80 °C, then AlBr_3 (213 mg, 0.8 mmol) was added. The reaction mixture was stirred for 4 h at 80 °C until it became blue, then it was cooled to room temperature, quenched with a 1N HBr solution and extracted with CHCl_3 (2x30mL). The combined organic phases were washed with brine, dried over anhydrous Na_2SO_4 and the solvent was removed under vacuum. The crude product was purified by column chromatography (silica gel, hexane) to give **11** as a white solid (297 mg, yield 88%). $R_f = 0.79$ (hexane); m.p. = 135-137 °C; ^1H -NMR (500 MHz, CDCl_3), δ (ppm): 7.59 (s, 1H); ^{13}C -NMR (126 MHz, CDCl_3), δ (ppm): 135.5, 135.5, 135.1, 134.7, 131.9, 129.2, 31.9; FTIR: $\tilde{\nu}_{\text{max}} = 1370, 1354, 1335, 1266, 1231, 1148, 963, 746, 735, 675, 667, 577, 490 \text{ cm}^{-1}$.

2,2'-((perchlorophenyl)methylene)bis(1,3,5-tribromobenzene) (7): A 15 mL pressure tube, equipped with a magnetic stirrer, was charged with **10** (100 mg, 0.3 mmol), 1,3,5-tribromobenzene (567 mg, 1.8 mmol) and AlCl_3 (44 mg, 0.33 mmol). The reaction mixture was heated at 120 °C under stirring until it became violet (1h), then it was cooled to room temperature, quenched with a 1N HCl solution and extracted with CHCl_3 (2x30mL). The combined organic phases were washed with brine and with a NaHCO_3 5% w/w solution, dried over anhydrous Na_2SO_4 and the solvent was removed under vacuum. The crude product was purified by column chromatography (silica gel, hexane) and crystallization with CHCl_3 /hexane 1:1 to give **7** as a white solid (52 mg). Mother liquors were furtherly crystallized in hexane affording an additional amount of **7** (90 mg). The target molecule was obtained in an overall yield of 53%. $R_f = 0.71$ (hexane); Darkening of the product was observed upon heating, m.p. = 315-317 °C; ^1H -NMR (500 MHz, CDCl_3), δ (ppm): 7.77 (d, $J = 2.1$ Hz, 1H), 7.74 (d, $J = 2.1$ Hz, 1H), 7.68 (d, $J = 2.1$ Hz, 1H), 7.65 (d, $J = 2.1$ Hz, 1H), 6.63 (s, 1H); ^{13}C -NMR (126 MHz, CDCl_3), δ (ppm): 137.3, 137.1, 137.1, 136.4, 136.3, 136.1, 135.7, 135.4, 134.8, 133.5, 133.5, 132.3, 128.5, 128.4, 127.5, 127.1, 122.2, 122.0, 60.6; FTIR: $\tilde{\nu}_{\text{max}} = 1561, 1530, 1421, 1365, 1351, 1295, 1231, 1218, 1113, 862, 853, 797, 760, 754, 728, 671 \text{ cm}^{-1}$.

6,6'-((perchlorophenyl)methylene)bis(3-bromo-1,2,4,5-tetrafluorobenzene) (8): A 25 mL two-necked round bottom flask, equipped with a reflux condenser and a magnetic stirrer, was charged with **11** (100 mg, 0.24 mmol) and 1-bromo-2,3,5,6-tetrafluorobenzene (300 μL , 2.48 mmol). This mixture was heated to 80 °C, then AlBr_3 (69 mg, 0.26 mmol) was added. The resulting mixture was stirred for 1h at 80 °C until it became blue, then it was quenched with a 1N HBr solution and extracted with CHCl_3 (2x30 mL). The combined organic phases were washed with a NaHCO_3 10% w/w solution, dried over anhydrous Na_2SO_4 and the solvent was removed under vacuum. The crude product was purified through column chromatography (silica gel, hexane) to give **8** as a sticky, white solid (86 mg, yield 50%); $R_f = 0.68$ (hexane); ^1H -NMR (500 MHz, CDCl_3), δ (ppm): 7.10 (s, 1H); ^{13}C -NMR (126 MHz, CDCl_3), δ (ppm): 146.4-144.0 (doublet of multiplets, $J \approx 250$ Hz), 144.42-144.09 (m), 135.4, 135.1, 133.3,

133.1, 115.2 (t, $J = 11.4$ Hz), 100.9 (tt, $J = 22.5$, 1.8 Hz), 35.1; FTIR: $\tilde{\nu}_{\max} = 1477, 1453, 1365, 1271, 966, 940, 836, 792, 684, 668, 607, 573$ cm⁻¹.

2,2'-((perchlorophenyl)methylene)bis(1,3,5-tribromobenzene) radical (12): A 50 mL three-necked round bottom flask, covered with aluminium foil and equipped with a magnetic stirrer, was charged with a solution of **7** (50 mg, 0.056 mmol) in 10 mL of anhydrous THF, under nitrogen atmosphere. A 56% w/w aqueous solution of tetrabutylammonium hydroxide (28 μ L, 0.059 mmol) was added to the reaction mixture that became immediately red for the carbanion formation. The resulting mixture stirred for 24 h at room temperature in the dark, then tetrachloro-1,4-benzoquinone (15 mg, 0.06 mmol) was added. After stirring for 5h, the reaction solvent was removed at reduced pressure and the crude product was purified by column chromatography (silica gel, hexane/dichloromethane 8:2) to give **12** as a red solid (41 mg, yield 82%). $R_f = 0.78$ (hexane/dichloromethane 8:2); Darkening of the product was observed upon heating, m.p. = 288-290 °C; HRMS (LC-IT-TOF, elution with methanol) m/z: M[•] calculated for C₁₉H₄Cl₅Br₆: 880.3861; found 880.3892; FTIR: $\tilde{\nu}_{\max} = 1544, 1505, 1353, 1332, 1263, 1178, 862, 855, 759, 732, 616$ cm⁻¹.

6,6'-((perchlorophenyl)methylene)bis(3-bromo-1,2,4,5-tetrafluorobenzene) radical (13): A 50 mL three-necked round bottom flask, covered with aluminium foil and equipped with a magnetic stirrer, was charged with a solution of **8** (20 mg, 0.028 mmol) in 10 mL of anhydrous THF, under nitrogen atmosphere. NaH (60% dispersion in mineral oil, 2.4 mg, 0.059 mmol) was added to the reaction mixture that became slowly orange for the carbanion formation. The resulting mixture was stirred for 2 h at room temperature in the dark, then tetrachloro-1,4-benzoquinone (15 mg, 0.059 mmol) was added (72h). The reaction solvent was removed at reduced pressure, and the crude product was purified by column chromatography (silica gel, hexane) to give **13** as a sticky, pale red solid (8 mg, yield 40%). $R_f = 0.65$ (hexane); HRMS (LC-IT-TOF, elution with methanol) m/z: M[•] calculated for C₁₉Br₂Cl₅F₈: 712.6687; found 712.6688; FTIR: $\tilde{\nu}_{\max} = 1481, 1466, 1367, 1339, 978, 970, 676$ cm⁻¹.

Computational details: Quantum chemical calculations with density functional theory (DFT) and time-dependent density functional theory (TDDFT) were carried out on **12**, **13** and, for comparison, on unsubstituted triphenylmethane (TPM) radical (see **Figure S19**). Two functionals were employed: the exchange-correlation B3LYP and the long-range corrected functional ω B97X-D, both in conjunction with the 6-31+G** basis set. Diffuse functions and additional polarization functions are important for heavy atoms. Equilibrium structures of the radicals were optimized in vacuo for both the ground state and the lowest excited state. Molecular orbitals were visualized with IQmol^[33]. The B3LYP functional was successfully employed to predict mixed-halide triphenyl methyl radicals^[22] while ω B97X-D was previously employed to investigate organic neutral radical emitters with charge transfer character^[14]. Vibrational frequency calculations at optimized geometries revealed no imaginary frequencies demonstrating that computed geometries correspond to global minima. Furthermore, the computed vibrational frequencies and IR intensities were compared to measured FTIR spectra (**Figures S20-S21**), displaying a close agreement with observed spectra. In addition, the Huang-Rhys parameters S_k for the $D_1 \rightarrow D_0$ transition^[34] were computed for each vibrational mode k with frequency ν_k . Each S_k was obtained as $S_k = \frac{1}{2} B_k^2$, where B_k is the dimensionless displacement parameter defined, assuming

the harmonic approximation as: $B_k = \sqrt{\frac{2\pi\nu_k}{h}} [X_j - X_i] M^{1/2} Q_k(j)$ where $X_{j,i}$ is the 3N dimensional vector of the Cartesian coordinates of the D_0 and D_1 structures, M is the 3N \times 3N diagonal matrix of atomic masses and $Q_k(j)$ is the 3N dimensional vector describing the ν_k normal coordinate of the D_0 state in terms of mass weighted Cartesian coordinates. All quantum chemical calculations were carried out with the Gaussian 16 suite of programs^[35].

Acknowledgements

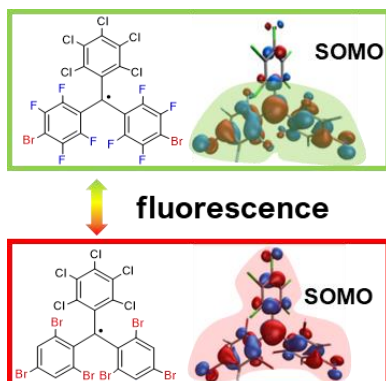
DM gratefully acknowledges the PON-RI Industrial Chemical and Molecular Sciences PhD XXXVII cycle action for funding, an initiative co-funded by European Union through the PON 2022-2025 for Green and Innovation topics (ID grant 634338). DB acknowledges the REFIN (Return for Future Innovation) action for funding, an initiative cofounded by European Union through the POR Puglia 2014-2020 (ID grant 2455F798). JK thanks the project CZ.02.2.69/0.0/0.0/18_053/0016962 of the Ministry of Education Youth and Sports of the Czech Republic. FN and YD acknowledge support from "Valutazione della Ricerca di Ateneo" (VRA) University of Bologna. YD acknowledges Ministero dell'Università e della Ricerca (MUR) for her Ph.D. fellowship.

Keywords: trityl radicals • doublet emitters • fluorinated compounds • open-shell species •

- [1] I. Ratera, J. Veciana, *Chem. Soc. Rev.* **2012**, *41*, 303–349.
- [2] R. Matsuoka, A. Mizuno, T. Mibu, T. Kusamoto, *Coord. Chem. Rev.* **2022**, *467*, 214616.
- [3] X. Bai, W. Tan, A. Abdurahman, X. Li, F. Li, *Dyes Pigm.* **2022**, *202*, 110260.
- [4] C. H. Liu, E. Hamzehpoor, Y. Sakai-Otsuka, T. Jadhav, D. F. Perepichka, *Angew. Chemie Int. Ed.* **2020**, *59*, 23030–23034.
- [5] P. Mayorga-Burrezo, V. G. Jiménez, D. Blasi, T. Parella, I. Ratera, A. G. Campaña, J. Veciana, *Chem. Eur. J.* **2020**, *26*, 3776–3781.
- [6] P. Mayorga Burrezo, V. G. Jiménez, D. Blasi, I. Ratera, A. G. Campaña, J. Veciana, *Angew. Chemie Int. Ed.* **2019**, *58*, 16282–16288.
- [7] J. F. Chen, G. Tian, K. Liu, N. Zhang, N. Wang, X. Yin, P. Chen, *Org. Lett.* **2022**, *24*, 1935–1940.
- [8] Y. Hattori, E. Michail, A. Schmiedel, M. Moos, M. Holzapfel, I. Krummenacher, H. Braunschweig, U. Müller, J. Pflaum, C. Lambert, *Chem. Eur. J.* **2019**, *25*, 15463–15471.
- [9] X. Wu, J. O. Kim, S. Medina, F. J. Ramírez, P. Mayorga Burrezo, S. Wu, Z. L. Lim, C. Lambert, J. Casado, D. Kim, J. Wu, *Chem. Eur. J.* **2017**, *23*, 7698–7702.
- [10] D. Blasi, D. M. Nikolaidou, F. Terenziani, I. Ratera, J. Veciana, *Phys. Chem. Chem. Phys.* **2017**, *19*, 9313–9319.
- [11] Y. Teki, K. Kato, S. Kimura, T. Kusamoto, H. Nishihara, *Angew. Chemie Int. Ed.* **2018**, 1–6.
- [12] S. Kimura, S. Kimura, K. Kato, Y. Teki, H. Nishihara, T. Kusamoto, *Chem. Sci.* **2021**, *12*, 2025–2029.
- [13] J. M. Hudson, T. J. H. Hele, E. W. Evans, *J. Appl. Phys.* **2021**, *129*, 180901.
- [14] H. Guo, Q. Peng, X. K. Chen, Q. Gu, S. Dong, E. W. Evans, A. J. Gillett, X. Ai, M. Zhang, D. Credgington, V. Coropceanu, R. H. Friend, J. L. Brédas, F. Li, *Nat. Mater.* **2019**, *18*, 977–984.
- [15] X. Ai, E. W. Evans, S. Dong, A. J. Gillett, H. Guo, Y. Chen, T. J. H. Hele, R. H. Friend, F. Li, *Nature* **2018**, *563*, 536–540.
- [16] L. Chen, M. Arnold, Y. Kittel, R. Blinder, F. Jelezko, A. J. C. Kuehne, *Adv. Opt. Mater.* **2022**, *10*, DOI

- 10.1002/adom.202102101.
- [17] M. Ballester, J. Riera, J. Castafier, C. Badía, J. M. Monsó, *J. Am. Chem. Soc.* **1971**, 93, 2215–2225.
- [18] M. Ballester, J. Riera, J. Castañer, C. Rovira, O. Armet, *Synth.* **1986**, 1986, 64–66.
- [19] S. Castellanos, D. Velasco, F. López-Calahorra, E. Brillas, L. Julia, *J. Org. Chem.* **2008**, 73, 3759–3767.
- [20] A. Heckmann, C. Lambert, *J. Am. Chem. Soc.* **2007**, 129, 5515–5527.
- [21] Y. Hattori, S. Tsubaki, R. Matsuoka, T. Kusamoto, H. Nishihara, K. Uchida, *Chem. Asian J.* **2021**, 16, 2538–2544.
- [22] L. Chen, M. Arnold, R. Blinder, F. Jelezko, A. J. C. Kuehne, *RSC Adv.* **2021**, 11, 27653–27658.
- [23] Y. Hattori, T. Kusamoto, H. Nishihara, *RSC Adv.* **2015**, 5, 64802–64805.
- [24] F. Babudri, A. Cardone, G. M. Farinola, F. Naso, T. Cassano, L. Chiavarone, R. Tommasi, *Macromol. Chem. Phys.* **2003**, 204, 1621–1627.
- [25] F. Babudri, A. Cardone, L. Chiavarone, G. Ciccarella, G. M. Farinola, F. Naso, G. Scamarcio, *Chem. Commun.* **2001**, 1940–1941.
- [26] J. Peeling, E. Ludger, T. Schaefer, *Can. J. Chemistry* **1974**, 52, 849–854.
- [27] J. Peeling, T. Schaefer, C. M. Wong, *Can. J. Chemistry* **1970**, 48, 2839–2842.
- [28] B. J. Fuhr, B. W. Goodwin, H. M. Hutton, T. Schaefer, *Can. J. Chemistry* **1970**, 48, 1558–1565.
- [29] H. Zhou, S. Wu, Y. Duan, F. Gao, Q. Pan, Y. Kan, Z. Su, *New J. Chem.* **2022**, DOI 10.1039/d2nj01548j.
- [30] A. Bromberg, D. Meisel, *J. Phys. Chem.* **1985**, 89, 2507–2513.
- [31] A. Szabo, N. L. Ostlund, in *Mod. Quantum Chem. Introd. to Adv. Electron. Struct. Theory*, Dover Publications, Inc., New York, **1996**.
- [32] S. R. Ruberu, M. A. Fox, *J. Phys. Chem.* **1993**, 97, 143–149.
- [33] A. Gilbert, **2020**, 2020.
- [34] F. Negri, M. Z. Zgierski, *J. Chem. Phys.* **1992**, 97, 7124–7136.
- [35] M. J. . Frisch, G. W. . Trucks, H. B. . Schlegel, G. E. . Scuseria, M. A. . Robb, J. R. . Cheeseman, G. . Scalmani, V. . Barone, G. A. . Petersson, H. . Nakatsuji, X. . Li, M. . Caricato, A. V. . Marenich, J. . Bloino, B. G. . Janesko, R. . Gomperts, B. . Mennucci, H. P. . Hratchian, J. V. . Ortiz, A. F. . Izmaylov, J. L. . Sonnenberg, D. . Williams-Young, F. . Ding, F. . Lipparini, F. . Egidi, J. . Goings, B. . Peng, A. . Petrone, T. . Henderson, D. . Ranasinghe, J. . Zakrzewski, V. G. . Gao, N. . Rega, G. . Zheng, W. . Liang, M. . Hada, M. . Ehara, K. . Toyota, R. . Fukuda, J. . Hasegawa, M. . Ishida, T. . Nakajima, Y. . Honda, O. . Kitao, H. . Nakai, T. . Vreven, K. . Throssell, J. . Montgomery, J. A., J. E. . Peralta, F. . Ogliaro, M. J. . Bearpark, J. J. . Heyd, E. N. . Brothers, K. N. . Kudin, V. N. . Staroverov, T. A. . Keith, R. . Kobayashi, J. . Normand, K. . Raghavachari, A. P. . Rendell, J. C. . Burant, S. S. . Iyengar, J. . Tomasi, M. . Cossi, J. M. . Millam, M. . Klene, C. . Adamo, R. . Cammi, J. W. . Ochterski, R. L. . Martin, K. . Morokuma, O. . Farkas, J. B. . Foresman, D. J. Fox, *Gaussian, Inc., Wallingford CT*, **2016**.

Entry for the Table of Contents



Two new mixed-halide trityl radicals bearing p-brominated positions were synthesized in good yield from halogenated triphenylmethanes obtained by multistep Friedel-Craft reactions. Their electrochemical and spectroscopic properties were reported as well as quantum-chemical calculations carried out to supplement the experimental investigation. The most blue-shifted emission among trityl radicals was achieved for the highly fluorinated trityl radical.

Institute and/or researcher Twitter usernames: <https://twitter.com/FarinolaGroup?t=lcX3n-kizSQMSeICzLIVyA&s=08>